Sensitivity of Austempering Heat Treatment of Ductile Irons to Changes in Process Parameters

A. D. Boccardo, P. M. Dardati, L. A. Godoy & D. J. Celentano

Metallurgical and Materials Transactions B

ISSN 1073-5615

Metall and Materi Trans B
DOI 10.1007/s11663-018-1222-y

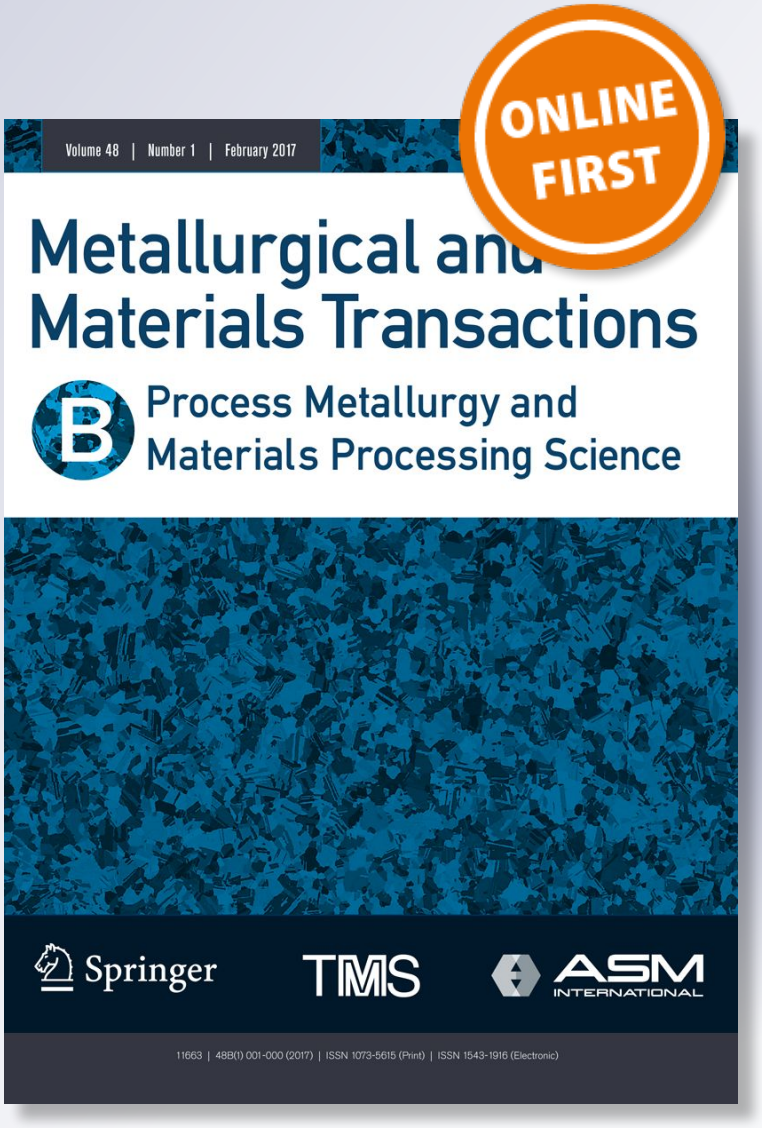

Springer

Sensitivity of Austempering Heat Treatment of Ductile Irons to Changes in Process Parameters

A.D. BOCCARDO, P.M. DARDATI, L.A. GODOY, and D.J. CELENTANO

Austempered ductile iron (ADI) is frequently obtained by means of a three-step austempering heat treatment. The parameters of this process play a crucial role on the microstructure of the final product. This paper considers the influence of some process parameters (*i.e.*, the initial microstructure of ductile iron and the thermal cycle) on key features of the heat treatment (such as minimum required time for austenitization and austempering and microstructure of the final product). A computational simulation of the austempering heat treatment is reported in this work, which accounts for a coupled thermo-metallurgical behavior in terms of the evolution of temperature at the scale of the part being investigated (the macroscale) and the evolution of phases at the scale of microconstituents (the microscale). The paper focuses on the sensitivity of the process by looking at a sensitivity index and scatter plots. The sensitivity indices are determined by using a technique based on the variance of the output. The results of this study indicate that both the initial microstructure and the thermal cycle parameters play a key role in the production of ADI. This work also provides a guideline to help selecting values of the appropriate process parameters to obtain parts with a required microstructural characteristic.

https://doi.org/10.1007/s11663-018-1222-y

I. INTRODUCTION

AUSTEMPERED ductile iron (ADI) is an metallic alloy with a microstructure at ambient temperature formed by graphite nodules inserted in a metallic matrix called ausferrite, the latter being a microconstituent formed by ferrite subunits embedded in austenite. Because of several advantages identified with the use of ADI, such as a wide range of mechanical properties, casting and machining simplicity, there is an increasing use of this material in the automotive and in the agricultural industries.

ADI can be obtained from a conventional ductile iron (DI) which is subsequently subjected to the so-called three-step austempering heat treatment.[1–3] The steps of this heat treatment are as follows: In the first step, the austenitization takes place in which the part is heated up and kept at the austenitizing temperature T_γ (1123 K (850 °C) $\leq T_\gamma \leq$ 1223 K (950 °C)) in order to transform the initial ferritic-pearlitic matrix into a completely austenitic matrix and with the appropriate carbon content. In the second step, the part is cooled down and kept at the austempering temperature T_A (523 K (250 °C) $\leq T_A \leq$ 723 K (450 °C)) to develop the austempering process. In the third step, the part is cooled down to the ambient temperature T_{amb}. The durations of the first and second steps are, respectively, called the austenitization (t_γ) and austempering (t_A) times, as shown in Figure 1.

In the three-step heat treatment, it is possible to identify parameters of different nature related to (a) the thermal cycle (austenitizing and austempering temperatures, austenitization and austempering times, cooling rate when the part is cooled down from T_γ to T_A), (b) the DI initial microstructure (including the graphite nodule count, type of initial matrix, and chemical composition), and (c) the part geometry; all of them having influence on the final microstructure of the ADI and, therefore, on the obtained mechanical properties. Thus, it is crucial to identify the influence of each

A.D. BOCCARDO is with the Instituto de Estudios Avanzados en Ingeniería y Tecnología, IDIT, CONICET-Universidad Nacional de Córdoba, Vélez Sarsfield 1611, Córdoba, X5000, Argentina and also with the Grupo de Investigación y Desarrollo en Mecánica Aplicada, GIDMA, Facultad Regional Córdoba, Universidad Tecnológica Nacional, Maestro M. Lopez esq. Cruz Roja Argentina, Córdoba, X5000, Argentina. Contact e-mail: aboccardo@frc.utn.edu.ar P.M. DARDATI is with the Grupo de Investigación y Desarrollo en Mecánica Aplicada, GIDMA, Facultad Regional Córdoba, Universidad Tecnológica Nacional. L.A. GODOY is with the Instituto de Estudios Avanzados en Ingeniería y Tecnología, IDIT, CONICET-Universidad Nacional de Córdoba and also with the Facultad de Ciencias Exactas, Físicas y Naturales, Universidad Nacional de Córdoba, Vélez Sarsfield 1611, Córdoba, X5000, Argentina. D.J. CELENTANO is with the Department of Mechanical and Metallurgical Engineering, Research Center for Nanotechnology and Advanced Materials (CIEN-UC), Pontificia Universidad Católica de Chile, Vicuña Mackenna 4860, Santiago de Chile, 7820436, Chile.

Manuscript submitted July 28, 2017.

Published online: 07 March 2018

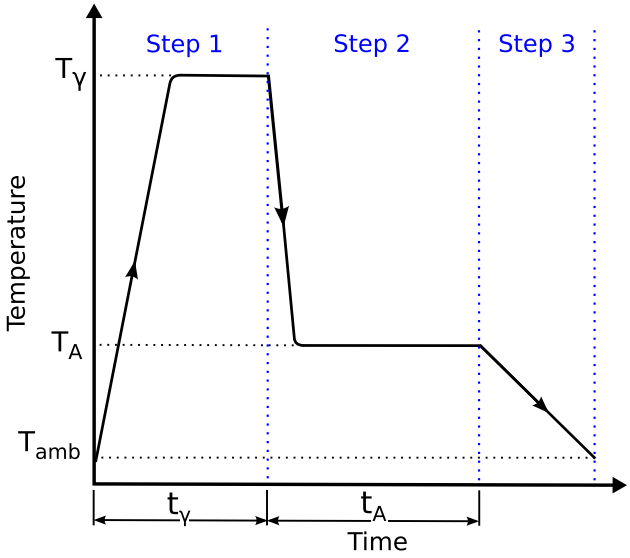

Fig. 1—Three-step austempering heat treatment.

parameter in order to adequately design the heat treatment leading to the ADI part.

Several researchers have addressed the influence of ADI parameters based on experiments. The influence of the chemical composition on the austemperability and kinetics of phase transformations was analyzed by Trudel and Gagné[4] and Bosnjak *et al.*.[5] The influence of austempering temperature on the kinetics of ausferritic transformation was studied by Bosnjak *et al.*[5] and Fraś *et al.*.[6] The influence of austenitizing and austempering temperatures on the mechanical properties and the final phase fractions was analyzed by Trudel and Gagné.[4] Finally, the influence of graphite nodule count on the kinetics of phase transformations was recently studied by Fraś *et al.*.[6] Due to limitations of resources available to carry out experiments, it has not been possible to perform sensitivity studies based on the results of References 4–6. As an alternative, a sensitivity analysis can be carried out by means of a numerical simulation of the austempering heat treatment, in the same way that this class of studies has been performed for different manufacture processes such as hot rolling,[7] arc welding,[8–10] metal extrusion,[11–13] and solidification.[14,15] There are several models that deal with the numerical simulation of the three-step austempering heat treatment such as References 16–18.

This work aims to identify the influence of specific process parameters, such as graphite nodule count, type of initial matrix, and austenitizing and austempering temperatures, on particular features of the heat process, such as the minimum required time for austenitization step (step 1) to obtain an austenitic matrix with homogeneous carbon content at austenitizing temperature (MRT_γ), the minimum required time for austempering step (step 2) to complete the ausferritic transformation (MRT_A), and the phase volume fractions of the ADI microstructure at the end of austempering heat treatment. In order to do that, the heat treatment is simulated by employing a coupled thermo-metallurgical model, and the results are subsequently analyzed using a variance-based sensitivity analysis tool and scatter plots.

II. AUSTEMPERING HEAT TREATMENT MODEL

The present model of austempering heat treatment considers the thermal and metallurgical aspects of the problem. The thermal aspect focuses on the evolution of the temperature in the part at the macroscale, whereas the metallurgical aspect considers the evolution of phases at the microscale level taking into account the type, shape, and size of the phases that form the DI microstructure.

The thermal model is solved by means of the finite element method implemented in an in-house finite element code, which has been validated in previous engineering applications (see References 17–21). At each Gauss point of the finite element mesh, the metallurgical model is solved by the explicit Euler method. This model considers a bidirectional coupling between the thermal and the metallurgical models that allows predicting the evolution of phases as a function of temperature and vice versa.

Assuming a known response at time t, the numerical solution at time $t + \Delta t$ is calculated by the algorithm schematically illustrated in Figure 2.

A. *Thermal Model*

The local governing equation describing the evolution of a quasi-steady process is the energy balance equation written in a Lagrangian description,[19] valid in $\Omega \times \Upsilon$, where Ω is the spatial configuration of a body and Υ denotes the time interval of interest with time $t \in \Upsilon$, as

$$\rho c \dot{T} = \nabla \cdot (\mathbf{k} \nabla \mathbf{T}) + \dot{Q}\,, \qquad [1]$$

where ρ is the density, c is the tangent specific heat capacity, Q is the heat generated due to phase changes, $\mathbf{k}$ is the isotropic conductivity tensor defined as $\mathbf{k} = k\mathbf{1}$, k is the conductivity coefficient, $\mathbf{1}$ is the unit tensor, and T is the temperature. In this equation, ∇ is the spatial gradient operator, and the superposed dot indicates time derivative. The material coefficients c and k are temperature-dependent.

The rate of the heat generation due to phase change is calculated as

$$\dot{Q} = \rho\left(L_{\alpha\to\gamma}\,\dot{f}_{\gamma_s} + L_{p\to\gamma}\,\dot{f}_{\gamma_m} + L_{\gamma\to\alpha}\,\dot{f}_{\alpha p}\right), \qquad [2]$$

where $L_{\alpha\to\gamma}$, $L_{p\to\gamma}$ and $L_{\gamma\to\alpha}$ are the latent heats of the stable and metastable reverse eutectoid transformations, and the ausferritic transformation, respectively. The volume fractions f_{γ_s}, f_{γ_m}, and $f_{\alpha p}$ correspond to stable and metastable austenite, and ferrite subunits, respectively.

The boundary condition imposed at the casting/environment interface is a Newton type law, valid in

$\Gamma_q x \Upsilon$, where Γ_q is the Ω contouring in which the condition is applied, written as

$$q_{conv} = -h(T - T_{env}), \quad [3]$$

where q_{conv} is the normal heat flux, h is the heat transfer coefficient at interface, and T and T_{env} are the temperatures at both sides of the interface.

B. *Metallurgical Model*

The metallurgical model simulates the phase transformations that occur through the three-step heat treatment, and is based on the metallurgical model presented by the authors[18] that was validated by comparison with experimental results. In this work, the stable (EITs) and metastable (EITm) reverse eutectoid, and the ausferritic (AT) transformations are considered. Moreover, the carbon homogenization in austenite (HA) at the austenitizing temperature is also taken into account. These transformations occur in specific stages of the heat treatment where their evolutions depend on the values of temperature, rate of temperature change, and phase fraction of the microconstituents. The algorithm of the metallurgical model that allows obtaining the final microstructure is illustrated in Figure 3, where T_{EITs}, T_{EITm}, and T_{AT} represent the temperatures at which the transformations EITs, EITm, and AT start, respectively. The temperatures T_{EITs} and T_{EITm} are calculated using the following equations[22]:

$$T_{\mathrm{EITs}} = 1012 + 31.5\mathrm{Si} - 7.7\mathrm{Cu} - 18.7\mathrm{Mn} + 3.3\mathrm{Mo} - 10.7\mathrm{Cr} - 26\mathrm{Ni} \quad [4]$$

$$T_{\mathrm{EITm}} = 1000 + 30.07\mathrm{Si} - 1.98\mathrm{Si}^2 - 10.7\mathrm{Cu} - 13.7\mathrm{Mn} + 9.3\mathrm{Mo} + 24.3\mathrm{Cr} - 12\mathrm{Ni}, \quad [5]$$

whereas T_{AT} is calculated as follows[23]:

$$T_{AT} = 1103 - 270\mathrm{C}_\gamma - 90\mathrm{Mn} - 37\mathrm{Ni} - 70\mathrm{Cr} - 83\mathrm{Mo}, \quad [6]$$

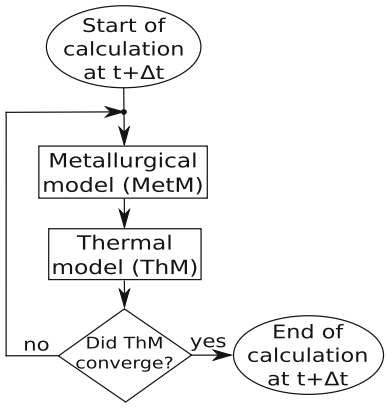

Fig. 2—Resolution scheme of the austempering heat treatment model at time $t + \Delta t$.

where Si, Cu, Mn, Mo, Cr, and Ni are the contents of silicon, copper, manganese, molybdenum, chromium, and nickel, respectively, in the ADI. Moreover, C_γ is the carbon content in the austenite after *HA*. The contents of alloying elements are in weight percent, and T_{EITs}, T_{EITm}, and T_{AT} are measured in K.

For each phase transformation, the microstructure of the material is described by a representative volume element (RVE), in which the temperature and the chemical composition, except for carbon, are assumed to be uniform. These representative volume elements allow modeling the phase change considering the type, shape, and size of phases that form the DI microstructure during the different stages of the heat treatment. The models for EITs and EITm are described in Section II–A–1, while those for HA and AT are described in Sections II–A–2 and II–A–3, respectively.

1. *Reverse eutectoid transformation*

When the austenitization step begins, the DI microstructure is formed by graphite nodules, ferrite halos, and pearlite colonies. The ferrite halos are transformed into austenite (γ_s) by means of the stable reverse eutectoid transformation. In order to simplify the study, the equations presented by Boccardo *et al.*[17] are rewritten by considering all graphite nodules of equal size. The spherical representative volume element RVEs is formed by a spherical graphite nodule surrounded by a shell of austenite and a shell of ferrite (see Figure 4). The austenite shell is formed, when the transformation starts, by means of an instantaneous nucleation. The graphite, ferrite, and austenite volume fractions are calculated as

$$f_{Gr} = \frac{4\pi}{3} N_{set} r_{Gr}^3 \quad [7]$$

$$f_{\gamma_s} = \frac{4\pi}{3} N_{set} \left(r_\gamma^3 - r_{Gr}^3 \right) \quad [8]$$

$$f_\alpha = \frac{4\pi}{3} N_{set} \left(r_\alpha^3 - r_\gamma^3 \right), \quad [9]$$

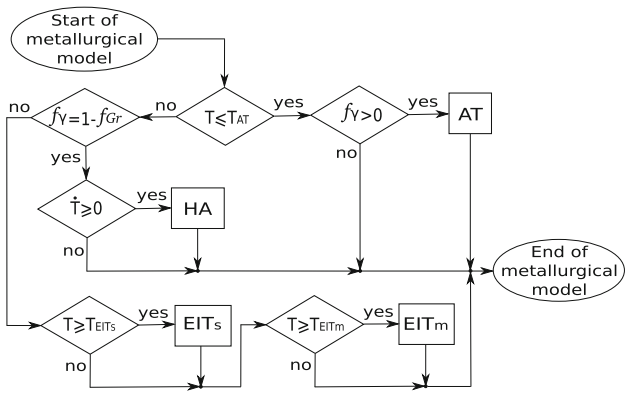

Fig. 3—Resolution scheme of the metallurgical model.

where r_{Gr} is the radius of the graphite nodule, r_γ is the radius of the austenite shell, and r_α is the size of RVEs. Moreover, N_{set} is the number of nodules per unit of volume. The size of the RVEs is calculated as $r_\alpha = r_{Gr_o}(1+f_{\alpha_0}/f_{Gr_0})^{1/3}$, where the subscript 0 applied to a variable denotes its value at the initial configuration Ω_0. The initial radius of graphite is equal to $r_{Gr_o} = [(3f_{Gr_o})/(4\pi N_{set})]^{1/3}$.

The growth rate of radii r_{Gr} and r_γ are evaluated employing the following system of ordinary differential equations, in which $r_{Gr}(0) = r_{Gr_o}$ and $r_\gamma(0) = 1.01 r_{Gr_o}$, as

$$\begin{cases} \dot{r}_{Gr} = \frac{D_\gamma \rho_\gamma r_\gamma}{r_{Gr}(r_\gamma - r_{Gr})} \frac{(c_{\gamma/\alpha} - c_{\gamma/Gr})}{(c_{Gr}\rho_{Gr} - c_{\gamma/Gr}\rho_\gamma)} \\ \dot{r}_\gamma = GI_E \left[\frac{D_\alpha \rho_\alpha r_\alpha}{r_\gamma(r_\alpha - r_\gamma)} \frac{(c_{\alpha_s} - c_{\alpha/\gamma})}{(c_{\gamma/\alpha}\rho_\gamma - c_{\alpha/\gamma}\rho_\alpha)} - \frac{D_\gamma \rho_\gamma r_{Gr}}{r_\gamma(r_\gamma - r_{Gr})} \frac{(c_{\gamma/\alpha} - c_{\gamma/Gr})}{(c_{\gamma/\alpha}\rho_\gamma - c_{\alpha/\gamma}\rho_\alpha)} \right] \end{cases}, \quad [10]$$

where D_α and D_γ are the diffusion coefficients of carbon in ferrite and austenite, respectively. The densities of graphite, ferrite, and austenite are denoted as ρ_{Gr}, ρ_α, and ρ_γ, respectively. Moreover c_{Gr}, $c_{\alpha/\gamma}$, c_{α_s}, $c_{\gamma/Gr}$, and $c_{\gamma/\alpha}$ stand for the carbon concentrations in graphite, ferrite in contact with austenite, ferrite places at the external surface of RVEs, austenite in contact with graphite, and austenite in contact with ferrite, respectively. All these parameters are calculated as in Reference 17. Additionally, GI_E is a nonlinear coefficient that considers the interaction of neighboring shells of austenite when this phase is growing and it is given by

$$\mathrm{GI_E} = \begin{cases} 1, & \text{for } (f_{\mathrm{Gr}} + f_{\gamma_s}) < f_{\mathrm{con}} \\ \left[\frac{1-(f_{\mathrm{Gr}}+f_{\gamma_s})}{(1-f_{\mathrm{con}})}\right]^{2/3}, & \text{for } (f_{\mathrm{Gr}} + f_{\gamma_s}) \geq f_{\mathrm{con}} \end{cases}, \quad [11]$$

where f_{con} is the sum of f_{Gr} and f_{γ_s} when the neighboring shells of austenite begin to be in contact and it is set to $f_{con} = 0.5$.

The pearlite is transformed into austenite (γ_m) by means of the metastable reverse eutectoid transformation. In order to simplify the study, the equations of Reference 17 are rewritten by considering that all pearlite colonies have equal interlaminar spacing size. The unidimensional representative volume element RVEm is formed by a half layer of cementite, a layer of austenite, and a half layer of ferrite (see Figure 5). When the transformation starts, the austenite layer is formed by means of an instantaneous nucleation. The volume fractions of pearlite and austenite are calculated as

$$f_p = f_{p_o}\left[1 - \frac{(x_\gamma - x_\theta)}{x_\alpha}\right] \quad [12]$$

$$f_{\gamma_m} = f_{p_o}\frac{(x_\gamma - x_\theta)}{x_\alpha}, \quad [13]$$

where x_θ and x_γ are the coordinates of the cementite-austenite and austenite-ferrite interfaces, respectively, and x_α is the size of RVEm. Furthermore, f_{p_o} is the initial pearlite volume fraction. The size of the RVEm is calculated as $x_\alpha = ips/2$, ips being the interlaminar spacing size of pearlite colonies.

The growth rates of the cementite-austenite and austenite-ferrite interfaces are evaluated by employing the following system of differential equations, in which $x_\theta(0) = x_{\theta_o}$ and $x_\gamma(0) = 1.01 x_{\theta_o}$, with $x_{\theta_o} = x_\alpha f_{\theta/p}$ where $f_{\theta/p} = 0.12$ is the volume fraction of cementite in a pearlite colony, as

$$\begin{cases} \dot{x}_\theta = \frac{D_\gamma \rho_\gamma}{(x_\gamma - x_\theta)} \frac{(c_{\gamma/\alpha} - c_{\gamma/\theta})}{(c_\theta \rho_\theta - c_{\gamma/\theta}\rho_\gamma)} \\ \dot{x}_\gamma = \frac{D_\alpha \rho_\alpha}{(x_\alpha - x_\gamma)} \frac{(c_{\alpha_m} - c_{\alpha/\gamma})}{(c_{\gamma/\alpha}\rho_\gamma - c_{\alpha/\gamma}\rho_\alpha)} - \frac{D_\gamma \rho_\gamma}{(x_\gamma - x_\theta)} \frac{(c_{\gamma/\alpha} - c_{\gamma/\theta})}{(c_{\gamma/\alpha}\rho_\gamma - c_{\alpha/\gamma}\rho_\alpha)} \end{cases}, \quad [14]$$

where ρ_θ is the cementite density. Moreover, c_{α_m}, c_θ, and $c_{\gamma/\theta}$ are the carbon concentrations in ferrite at x_α, cementite, and austenite in contact with cementite, respectively. All these parameters are calculated as in Reference 17.

The total austenite volume fraction resulting from the reverse eutectoid transformation is evaluated as

$$f_\gamma = f_{\gamma_s} + f_{\gamma_m}. \quad [15]$$

2. *Carbon homogenization in austenite*

The carbon concentration of austenite in equilibrium with graphite increases as the austenitizing temperature increases. This equilibrium carbon concentration in austenite is reached by means of carbon diffusion from graphite nodule to austenite through the graphite-austenite interface, and this process modifies the graphite nodule size. In order to simplify the study, the equations presented by Boccardo *et al.*[18] are rewritten by considering all graphite nodules of equal size. The spherical representative volume element RVEh is formed by a spherical graphite nodule surrounded by a shell of austenite (see Figure 6). The volume fractions of these phases are

$$f_{Gr} = \frac{4\pi}{3} N_{set} r_{Gr}^3 \quad [16]$$

$$f_\gamma = \frac{4\pi}{3} N_{set}\left(r_{shell}^3 - r_{Gr}^3\right), \quad [17]$$

where $r_{shell} = [(3/4\pi)/N_{set}]^{1/3}$ is the size of RVEh.

The growth rate of radius r_{Gr} is calculated by employing the following differential equation, in which $r_{Gr}(0) = r_{Gr_{o'}}$, where $r_{Gr_{o'}}$ is the graphite nodule radius when the reverse eutectoid transformation ends:

$$\dot{r}_{Gr} = \frac{D_\gamma \rho_\gamma r_{shell}}{r_{Gr}(r_{shell} - r_{Gr})} \frac{(c_{\gamma_{sh}} - c_{\gamma/Gr})}{(c_{Gr}\rho_{Gr} - c_{\gamma/Gr}\rho_\gamma)}, \quad [18]$$

where $c_{\gamma_{sh}}$ is the austenite carbon concentration at r_{shell}, and it is calculated by taking into account the carbon mass conservation in the RVEh.

3. *Ausferritic transformation*

During the ausferritic transformation, a fraction of austenite transforms into ferrite subunits. In order to

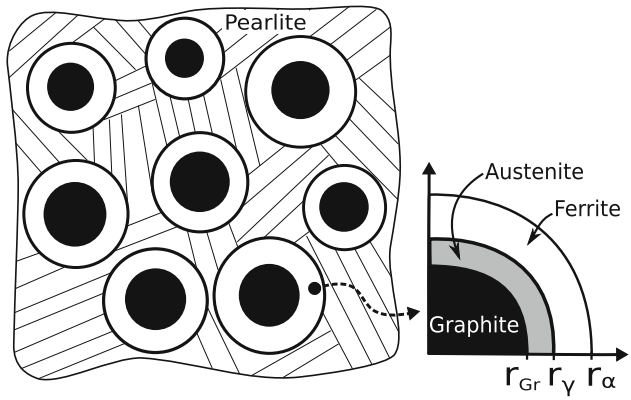

Fig. 4—Representative volume element RVEs employed to model the stable reverse eutectoid transformation.

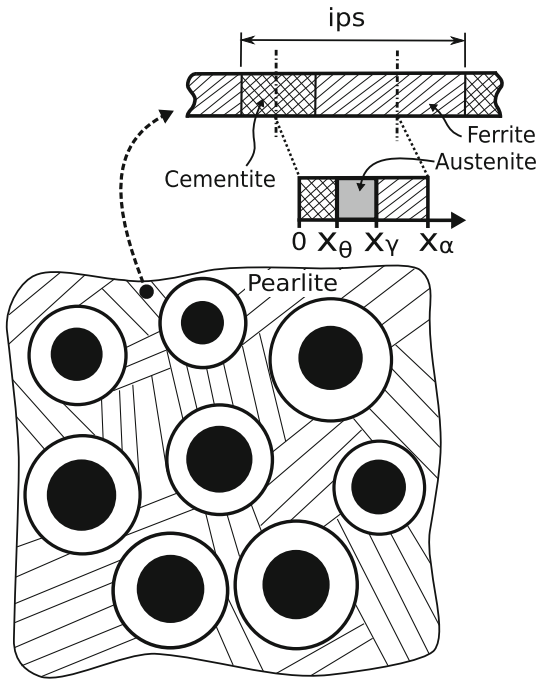

Fig. 5—Representative volume element RVEm employed to model the metastable reverse eutectoid transformation.

simplify the study, the equations presented by Boccardo *et al.*[24] are rewritten by considering all graphite nodules of equal size. The spherical RVEa is formed by a spherical graphite nodule surrounded by a shell of ausferrite and a shell of austenite (see Figure 7). The ausferrite is a microconstituent formed by austenite film, austenite block, and ferrite subunits. The ferrite subunits are formed by means of a continuous nucleation. The graphite nodule volume fraction remains constant during the transformation, while the ausferrite and austenite volume fractions are calculated as

$$f_{Ausf} = \frac{4\pi}{3} N_{set} \left(r_A^3 - r_{Gr}^3 \right) \quad [19]$$

$$f_\gamma = f_{\gamma_f} + f_{\gamma_b} + f_{\gamma_{sh}}, \quad [20]$$

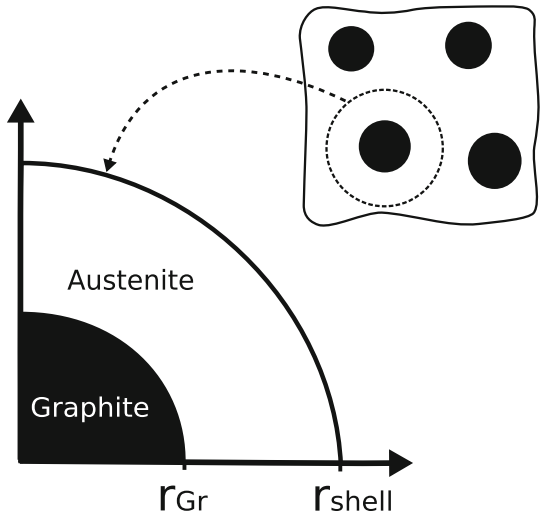

Fig. 6—Representative volume element RVEh proposed to model the carbon homogenization in austenite.

where r_A is the radius of ausferrite shell, and f_{γ_f}, f_{γ_b}, and $f_{\gamma_{sh}}$ are the austenite film, austenite block, and austenite shell volume fractions, respectively, which are evaluated as

$$f_{\gamma_f} = x_{\gamma f/\alpha p} f_{\alpha p} \quad [21]$$

$$f_{\gamma_b} = \frac{4\pi}{3} N_{set} \left(r_A^3 - r_{Gr}^3 \right) - f_{\alpha p} \left(1 + x_{\gamma f/\alpha p} \right) \quad [22]$$

$$f_{\gamma_{sh}} = \frac{4\pi}{3} N_{set} \left(r_{shell}^3 - r_A^3 \right), \quad [23]$$

where $f_{\alpha p}$ is the volume fraction of ferrite subunits. Moreover, $x_{\gamma f/\alpha p} = 0.12$ is the ratio between the volume fractions of the austenite film and ferrite subunits.

The growth rate of radius r_A and fraction $f_{\alpha p}$ are evaluated by using the following system of differential equations, in which $r_A(0) = r_{Gr_{o''}}$ and $f_{\alpha p}(0) = 0$, where

$r_{Gr_{o''}}$ is the graphite radius when the ausferritic transformation begins:

$$\begin{cases} \dot{r}_A = GI_A \frac{l_{\alpha p}}{t_{inc}} \\ \dot{f}_{\alpha p} = \frac{v_{\alpha p} N_{\alpha ps}^{ext}}{vol_{RVEa} t_{inc}} \left[1 - \frac{3 f_{\alpha p}}{4\pi N_{set} \zeta \left(r_A^3 - r_{Gr}^3 \right)} \right] \end{cases}, \quad [24]$$

where $l_{\alpha p}$ and $v_{\alpha p}$ are the length and volume of a ferrite subunit, respectively, t_{inc} is the incubation time of a set of ferrite subunits, $N_{\alpha ps}^{ext}$ is the number of subunits of a set of ferrite subunits, $vol_{RVEa} = (4/3)\pi r_{shell}^3$ is the volume of RVEa; and ζ is the volume fraction of ferrite subunits, with respect to the ausferrite volume fraction, when the ausferritic transformation ends. All these parameters are calculated as in Reference 24. Moreover, GI_A is a nonlinear coefficient that considers the interaction of neighboring shells of ausferrite when they are growing, and it is given by

$$GI_A = \begin{cases} 1, & for \quad (f_{Gr} + f_{Ausf}) < f_{con} \\ \left[\frac{1-(f_{Gr}+f_{Ausf})}{(1-f_{con})} \right]^{2/3}, & for \quad (f_{Gr} + f_{Ausf}) \geq f_{con} \end{cases}, \quad [25]$$

where f_{con} is the sum of f_{Gr} and f_{Ausf} when the neighboring shells of ausferrite begin to be in contact and it is set to $f_{con} = 0.5$.

III. SENSITIVITY ANALYSIS

In this paper, the sensitivity analysis is performed using the global variance-based sensitivity analysis tool developed by Saltelli *et al.*[25,26] This tool considers the model as a black box of the form $Y = f(X_1, X_2, \ldots, X_i, \ldots, X_q)$, where Y is the model output obtained for an input of q parameters.

The expected reduction in the variance of the model output that could be obtained if the value of a parameter X_i is fixed and the values of the remaining parameters $X_{\sim i}$ vary, is denoted as $V_{X_i}(E_{X_{\sim i}}(Y|X_i))$. Because the obtained reduction depends on the value at which X_i is fixed, $V_{X_i}(E_{X_{\sim i}}(Y|X_i))$ is calculated for all possible values of X_i. Regarding to this variance reduction, a first order sensitivity index is defined as

$$S_i = \frac{V_{X_i}(E_{X_{\sim i}}(Y|X_i))}{V(Y)}, \quad [26]$$

where $V(Y)$ is the variance of the model output Y.

The index S_i varies between zero and one, and it refers to the influence of X_i on the variance of the output considering no interaction between parameters. If S_i is close to one, the parameter X_i is very important because the obtained reduction $V_{X_i}(E_{X_{\sim i}}(Y|X_i))$ is close to $V(Y)$ when X_i is fixed. On the other hand, if S_i is close to zero, the parameter X_i does not play a key role in the variation of the output model, because the obtained reduction $V_{X_i}(E_{X_{\sim i}}(Y|X_i))$ is close to zero when X_i is fixed.

The expected reduction in the variance of the model output that could be obtained if the values of parameters $X_{\sim i}$ are fixed, that means when only the value of X_i varies, is denoted as $V_{X_{\sim i}}(E_{X_i}(Y|X_{\sim i}))$. Because this reduction in the variance depends on the values at which $X_{\sim i}$ are fixed, $V_{X_{\sim i}}(E_{X_i}(Y|X_{\sim i}))$ is calculated for all possible values of $X_{\sim i}$. In relation to this variance reduction, the so-called total effect index is defined as

$$S_{Ti} = 1 - \frac{V_{X_{\sim i}}(E_{X_i}(Y|X_{\sim i}))}{V(Y)}. \quad [27]$$

The index S_{Ti} varies between zero and one, and it refers to the influence of X_i on the variance of the output considering also the interaction between X_i and $X_{\sim i}$. If S_{Ti} is close to one it indicates that the parameter X_i plays a important role, because the obtained reduction $V_{X_{\sim i}}(E_{X_i}(Y|X_{\sim i}))$ is small when $X_{\sim i}$ are fixed. On the other hand, if $S_{Ti} = 0$ means that X_i does not have an influence on the model output.

The index defined as $S_{Ii} = (S_{Ti} - S_i)$ quantifies the interaction of X_i with $X_{\sim i}$, whose value varies between zero and one, such that $S_{Ii} = 1$ if X_i has a strong interaction with at least one other parameter, and $S_{Ii} = 0$ if X_i does not interact with other parameters. Moreover, the index $S_{TI} = (1 - \sum_{i=1}^{q} S_i)$ allows to identify how strong or weak is the influence of interactions among parameters on the variance of the output model. This index varies between zero and one, such that $S_{TI} = 1$ if the influence of interactions is strong and $S_{TI} = 0$ if there is no influence (because there is no interaction among parameters).

The mentioned indices are calculated employing the following equations, see Saltelli *et al.*[25,26]:

$$S_i = \frac{\frac{1}{N}\sum_{j=1}^{N} \left[y_A^{(j)} \left(y_{C_i}^{(j)} - y_B^{(j)} \right) \right]}{\frac{1}{N}\sum_{j=1}^{N} \left(y_A^{(j)} \right)^2 - \frac{1}{N^2}\sum_{j=1}^{N} \left(y_A^{(j)} \right) \sum_{j=1}^{N} \left(y_B^{(j)} \right)} \quad [28]$$

$$S_{Ti} = \frac{\frac{1}{2N}\sum_{j=1}^{N} \left(y_B^{(j)} - y_{C_i}^{(j)} \right)^2}{\frac{1}{N}\sum_{j=1}^{N} \left(y_A^{(j)} \right)^2 - \left[\frac{1}{N}\sum_{j=1}^{N} \left(y_A^{(j)} \right) \right]^2}, \quad [29]$$

where $y_A^{(j)}$, $y_B^{(j)}$, and $y_{C_i}^{(j)}$ are the elements j of the output vectors Y_A, Y_B, and Y_{C_i}, with $i = 1, \ldots, q$.

Elements j of vectors Y_A, Y_B, and Y_{C_i} are obtained by simulating the heat treatment with the model described in Section II. The different combinations of the parameter values employed in the simulations are placed in the row j of input matrices A, B, and C_i, respectively. The matrices A and B of dimension $N \times q$, where N is the base sample, are defined as

$$A = \begin{bmatrix} a_1^{(1)} & a_2^{(1)} & \cdots & a_i^{(1)} & \cdots & a_q^{(1)} \\ a_1^{(2)} & a_2^{(2)} & \cdots & a_i^{(2)} & \cdots & a_q^{(2)} \\ \vdots & \vdots & & \vdots & & \vdots \\ a_1^{(j)} & a_2^{(j)} & \cdots & a_i^{(j)} & \cdots & a_q^{(j)} \\ \vdots & \vdots & & \vdots & & \vdots \\ a_1^{(N)} & a_2^{(N)} & \cdots & a_i^{(N)} & \cdots & a_q^{(N)} \end{bmatrix} \quad [30]$$

$$B = \begin{bmatrix} b_1^{(1)} & b_2^{(1)} & \cdots & b_i^{(1)} & \cdots & b_q^{(1)} \\ b_1^{(2)} & b_2^{(2)} & \cdots & b_i^{(2)} & \cdots & b_q^{(2)} \\ \vdots & \vdots & & \vdots & & \vdots \\ b_1^{(j)} & b_2^{(j)} & \cdots & b_i^{(j)} & \cdots & b_q^{(j)} \\ \vdots & \vdots & & \vdots & & \vdots \\ b_1^{(N)} & b_2^{(N)} & \cdots & b_i^{(N)} & \cdots & b_q^{(N)} \end{bmatrix}, \quad [31]$$

where the components of the matrices are defined in this work as $a_i^{(j)} = f_i + \Delta f_i qr_i^{(j)}$ and $b_i^{(j)} = f_i + \Delta f_i qr_{q+i}^{(j)}$, where $qr_i^{(j)}$ and $qr_{q+i}^{(j)}$ are the components of a matrix $QR(N, 2q)$, whose elements vary in a quasi-random form between zero and one,[27] f_i is the minimum value of a parameter X_i ($f_i = f_{min_i}$), and Δf_i is defined as $\Delta f_i = (f_{max_i} - f_{min_i})$, f_{max_i} being the maximum value of a parameter X_i.

The input matrix C_i is assembled by replacing the column i of matrix B by the column i of matrix A as

$$C_i = \begin{bmatrix} b_1^{(1)} & b_2^{(1)} & \cdots & a_i^{(1)} & \cdots & b_q^{(1)} \\ b_1^{(2)} & b_2^{(2)} & \cdots & a_i^{(2)} & \cdots & b_q^{(2)} \\ \vdots & \vdots & & \vdots & & \vdots \\ b_1^{(j)} & b_2^{(j)} & \cdots & a_i^{(j)} & \cdots & b_q^{(j)} \\ \vdots & \vdots & & \vdots & & \vdots \\ b_1^{(N)} & b_2^{(N)} & \cdots & a_i^{(N)} & \cdots & b_q^{(N)} \end{bmatrix}. \quad [32]$$

IV. CASES OF STUDY

In order to study the influence of the process parameters, numerical simulations of the austempering heat treatment were performed for $N(2 + q)$ cases (with $N = 2100$ and $q = 4$). Parameters such as chemical composition (3.70C-2.65Si-0.1Mn-0.02P-0.01S-0.04Mg in weight per cent) and geometry of samples (cylindrical samples of $\varnothing 1.5mm \times 20mm$) were fixed to the values reported in the experimental work of Fraś *et al.*.[6] The interlaminar spacing of the pearlite colonies was set to ips = 0.5×10^{-5} m (coarse interlaminar spacing) because, according to previous studies presented by Boccardo,[28] it does not have a significant influence on the analyzed output.

To carry out the simulations of the thermal problem by means of the finite element method, and taking into account the symmetry of the cylindrical specimen, a geometry corresponding to 1/2 sample was meshed using 600 axisymmetric elements of four nodes (6 × 100 elements in the radial and axial directions, respectively), see Figure 8. The number of elements was obtained by means of convergence studies. The thermal boundary conditions were normal heat flux equal to zero at edges 1 and 2, and convection at edges 3 and 4. The average heat transfer coefficient is $h = 70\ W/m^2K$ during all the heating up and the cooling down from T_A to T_{amb}, whereas $h = 400\ W/m^2K$ during the cooling down from T_γ to T_A, values fitted from experimental data presented by Fraś *et al.*.[6] The DI thermal properties are shown in Table I. Regarding to the resolution of the metallurgical model, parameters such as coefficients of carbon diffusion, density of phases, carbon concentration in phases, and length and volume of ferrite subunits were set by employing the values reported by Boccardo *et al.*.[17,24] Moreover, the constants related to the ausferritic transformation model were fitted for the above-mentioned chemical composition employing the technique presented in Reference 24, resulting $k_1 = 1.33 \times 10^{15}$ and $k_2 = 4.7 \times 10^3$ J/mol.

The process parameters varied in this study are related to DI initial microstructure and thermal cycle, which are shown in Table II. The range of variation for each parameter was set according to values reported in References 5, 6, and 30, and are presented in Table III. In this analysis, the initial ferrite volume fraction $f_{\alpha_{0n}}$ is normalized with respect to the matrix volume fraction. The normalized initial pearlite volume fraction was evaluated as $f_{p_{0n}} = (1 - f_{\alpha_{0n}})$ and the initial volume fraction of graphite was calculated by taking into account the carbon mass conservation in the DI.

V. RESULTS AND DISCUSSION

The influence of process parameters was analyzed in this study based on the outputs presented in Table II and illustrated in Figure 9. The influence of each parameter was studied by means of a sensitivity analysis, and the behavior of the output was analyzed by employing scatter plots. The indices S_i and S_{Ti} are presented in Table IV, while the indices S_{Ii} and S_{TI} are presented in Table V.

The evolution of austenite and ferrite subunit volume fractions for different values of input parameters, which are shown in Table VI, are presented in Figure 10. Significant variations were observed in both phase evolutions during the step 2 and final phase fractions. For the cooling down from T_γ to T_A, the cooling rate is defined as CR = $(1073 - 873)\text{K}/\Delta t_{cd}$, where Δt_{cd} is the time to cooling the sample from 1073 K to 873 K. It is varied in the range of $45 < CR < 65$ K/s due to the different values of austenitizing and austempering temperatures considered in the study.

A. *Austenitization Step*

The minimum required time for step 1 (or austenitization step) is defined as the minimum time to obtain an

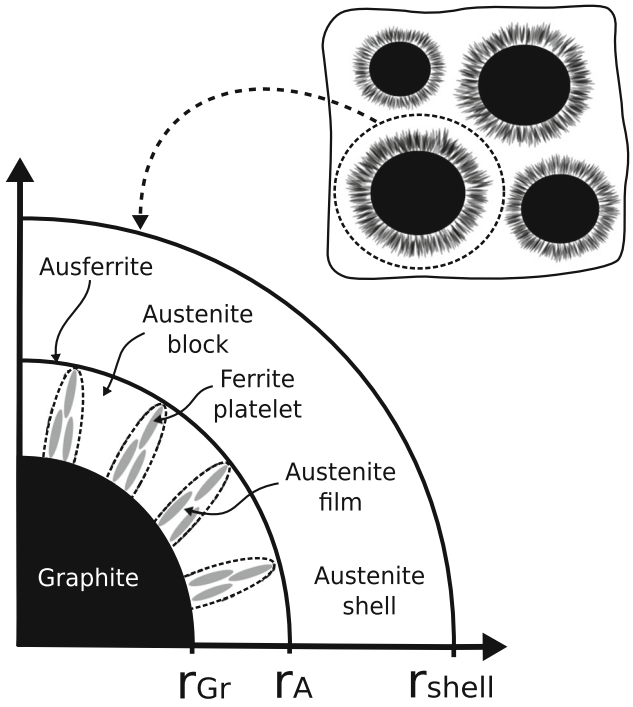

Fig. 7—Representative volume element RVEa employed to model the ausferritic transformation.

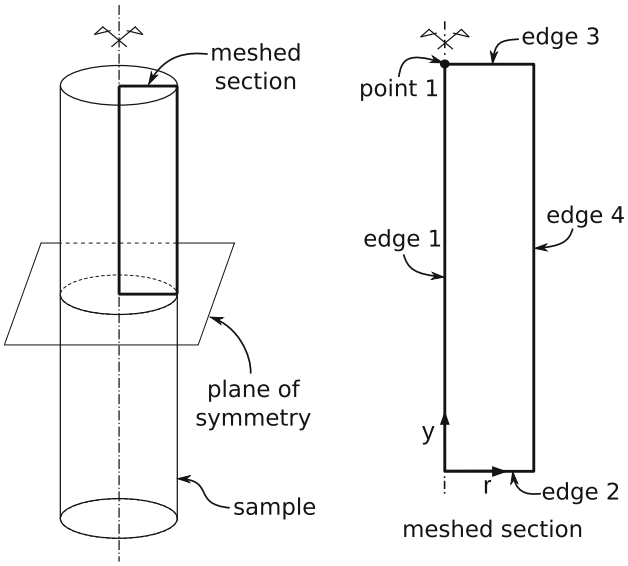

Fig. 8—Modeled geometry and thermal boundary conditions of the cylindrical sample.

austenitic matrix with homogeneous carbon content at the austenitizing temperature. It was computed as $MRT_\gamma = (t_{f_{\gamma max}} - t_{S1})$, where $t_{f_{\gamma max}}$ is the time to get the maximum austenite volume fraction, which occurs for an austenitic matrix with homogeneous carbon content, and $t_{S1} = 0s$ is the time at which step 1 started.

Analyzing the total effect index S_{Ti} (Table IV), it could be observe that MRT_γ depends mainly on the austenitizing temperature. In the other hand, the graphite nodule count and type of initial matrix had a smaller influence. As was expected, the austempering temperature did not have an influence because it is not a parameter of the austenitization step. According to the value of S_{Ii}, the interaction between parameters was weak and it was confirmed with a value of S_{TI} close to zero.

MRT_γ is the sum of (a) time to get T_γ from T_{amb} and (b) time to transform the initial matrix into an austenitic matrix with homogeneous carbon content. The time to get T_γ increased when the value of this temperature increased, because longer heating time was required. Moreover, the time to transform the initial matrix decreased when T_γ increased, N_{set} increased, and $f_{\alpha_{0n}}$ decreased. This occurred because an increment of T_γ increased the coefficient of carbon diffusion, and an increment of N_{set} decreased the size of RVEs and it helped to reach carbon homogenization. Additionally, a decrement of $f_{\alpha_{0n}}$ reduced the time to transform the initial matrix, because the transformation of ferrite into austenite required more time that the transformation of pearlite into austenite.

The values of MRT_γ, for all the simulations, are shown in scatter plots in Figure 11 as a function of the austenitizing temperature, initial volume fraction of ferrite, and graphite nodule count. The behavior of MRT_γ for some values of the analyzed process parameters has been indicated in dash line.

The results of the present model were compared with experimental results presented by Fraś *et al.*[6] and Boccardo *et al.*[18] As it is observed in Figure 12, MRT_γ tended to increase when the graphite nodule count decreased.

When there is a nonuniform distribution of graphite nodule sizes, MRT_γ also depends on the size of graphite nodules and their numbers. The influence of these parameters was analyzed for a few samples, which were

Table I. Thermal Properties of Ductile Iron[21,29,30]

Temperature [K (°C)]	Conductivity (W/m K)	Specific Heat (J/kg K)
293 (20)	44.1	500
553 (280)	44.1	612
693 (420)	40.9	672
833 (560)	37.1	732
973 (700)	33.6	750
1113 (840)	28.1	758
1253 (980)	22.5	786
ρ (kg/m^3)	7000	
Latent heat (J/kg)	$L_{p\to\gamma} = 1.28 \times 10^4$ $L_{\gamma\to\alpha} = 5.8 \times 10^4$	$L_{\alpha\to\gamma} = 5.8 \times 10^4$

Table II. Inputs and Outputs Considered in the Sensitivity Analysis

Input Parameter	N_{set}: Graphite nodule count
	$f_{\alpha_{0n}}$: Normalized ferrite volume fraction
	T_γ: Austenitizing temperature
	T_A: Austempering temperature
Output	MRT_γ: Minimum required time for step 1
	MRT_A: Minimum required time for step 2
	$f_{Gr_{end}}$: Final graphite volume fraction
	$f_{\alpha p_{end}}$: Final ferrite subunit volume fraction
	$f_{\gamma_{end}}$: Final austenite volume fraction

characterized by $f_{\alpha_{0n}} = 0.5$, $T_\gamma = 1223$ K (950 °C), $T_A = 623$ K (350 °C), and two sets of graphite nodules. The radii of graphite nodules for set 1 and set 2 were the smallest ($r_{Gr_1} = 6.04 \times 10^{-6}$ m) and the largest ($r_{Gr_2} = 1.47 \times 10^{-5}$ m) ones considered in the case of uniform graphite nodule size, respectively. The number of graphite nodules of each set was varied by modifying the initial normalized graphite volume fraction that is defined as $f_{Gr_{i_n}} = f_{Gr_i}/f_{Gr}$, where f_{Gr_i} is the graphite volume fraction of a set $i = 1, 2$, such that $f_{Gr_{1_n}} + f_{Gr_{2_n}} = 1$. The value of MRT_γ decreased when $f_{Gr_{1_n}}$ increased, because the number of graphite nodules with small size increased. The maximum and minimum values of MRT_γ were obtained for $f_{Gr_{1_n}} = 0$ (all graphite nodules of $r_{Gr_2} = 1.47 \times 10^{-5}$ m) and $f_{Gr_{1_n}} = 1$ (all graphite nodules of $r_{Gr_1} = 6.04 \times 10^{-6}$ m), respectively, as shown in Figure 13. A small difference between the minimum and maximum values was observed, because the graphite nodule size had low influence on MRT_γ.

B. *Austempering Step*

The minimum required time for step 2 (or austempering step) is defined as the minimum time to complete the ausferritic transformation. It was computed as $MRT_A = (t_{f_{\alpha p_{max}}} - t_{S2})$, where $t_{f_{\alpha p_{max}}}$ is the time to get the maximum ferrite subunit volume fraction and t_{S2} is the time at which step 2 started. When this maximum fraction is reached, the martensitic transformation does not start at ambient temperature because the austenite carbon concentration is large enough. Moreover, the carbide precipitation into the austenite starts after the window period, that means for time $t > MRT_A$.[23]

Analyzing the total effect index S_{Ti} (Table IV), it may be seen that MRT_A depended mainly on the

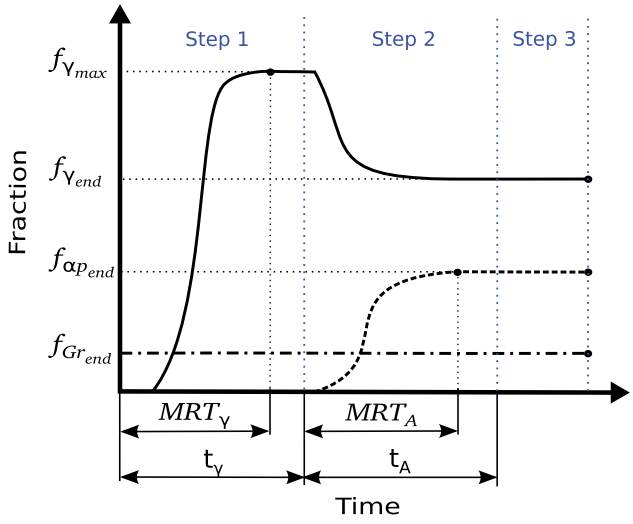

Fig. 9—Considered output in the sensitivity analysis.

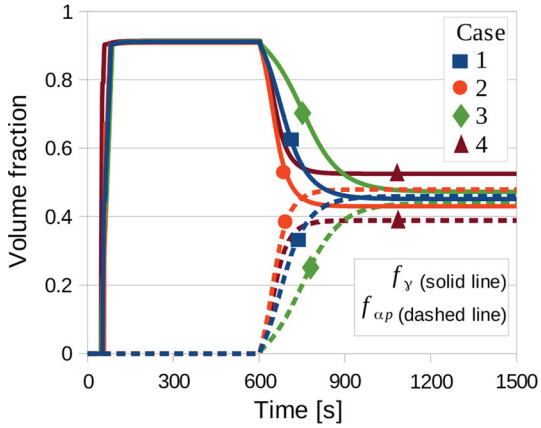

Fig. 10—Evolution of austenite and ferrite subunit volume fractions for different values of input parameters.

Table III. Range of Variation of Input Parameters

i	Parameter	f_{min_i}	f_{max_i}
1	N_{set} (nod/m^3)	8×10^{12}	1.18×10^{14}
2	$f_{\alpha_{0n}}$	0	1
3	T_γ $[K\ (^\circ C)]$	1143 (870)	1223 (950)
4	T_A $[K\ (^\circ C)]$	573 (300)	703 (430)

Table IV. S_i and S_{Ti} Indices for the Analyzed Output

Output	S_i				S_{Ti}			
	$f_{\alpha_{0n}}$	N_{set}	T_γ	T_A	$f_{\alpha_{0n}}$	N_{set}	T_γ	T_A
MRT_γ	0.05	0.07	0.81	0.0	0.08	0.08	0.84	0.0
MRT_A	0.0	0.19	0.0	0.71	0.0	0.22	0.04	0.79
$f_{Gr_{end}}$	0.0	0.0	1.0	0.0	0.0	0.0	1.0	0.0
$f_{\alpha p_{end}}$	0.0	0.0	0.88	0.13	0.0	0.0	0.87	0.14
$f_{\gamma_{end}}$	0.0	0.0	0.87	0.13	0.0	0.0	0.88	0.12

austempering temperature and graphite nodule count. On the other hand, the austenitizing temperature had lesser importance. According to S_{Ii}, there were small interactions between T_A and N_{set}, and T_A and T_γ.

MRT_A is the sum of (a) time to get T_A from T_γ and (b) time to transform austenite into ferrite subunits. The time to get T_A increased when T_A decreased and T_γ increased, because longer cooling time was required. Moreover, the time to transform austenite into ferrite subunits decreased when T_A increased, N_{set} increased, and T_γ decreased. This occurred because an increment of T_A incremented the austempering transformation rate due to an increment in the size of subunits, and also because an increment of N_{set} incremented the austempering transformation rate due to the formation of ferrite subunits at the graphite surface became more important than the formation at tips of ferrite subunits, the former having the shortest incubation time. Additionally, an increment of T_γ decreased the austempering transformation rate, because the carbon concentration at the beginning of the ausferritic transformation was increased, and this fact lengthened the incubation time of ferrite subunits.

The values of MRT_A, for all the simulations, are shown in scatter plots in Figure 14 as a function of the austempering temperature, graphite nodule count, and austenitizing temperature. The behavior of MRT_A for some values of process parameters has been indicated in dash line.

The model results were compared with experimental results presented by Fraś *et al.*[6] and Boccardo *et al.*[18] As it is observed in Figure 15, MRT_A tended to increase when the austempering temperature and graphite nodule count decreased.

When there is a nonuniform distribution of graphite nodule sizes, MRT_A also depends on both size and number of graphite nodules. The influence of these parameters was analyzed as for MRT_γ. The value of MRT_A remains almost constant when $f_{Gr_{1_n}}$ increases up to 0.75, and then decreases when $f_{Gr_{1_n}}$ tends to one, as shown in Figure 16. There was a remarkable difference between the minimum and maximum values, because the graphite nodule size is a parameter that influences on MRT_A.

C. *Phase Volume Fractions at the End of the Heat Treatment*

The volume fraction $f_{Gr_{end}}$ was only influenced by the austenitizing temperature, as it follows from the values of S_{Ti} in Table IV. As a consequence, there was no interaction between the process parameters ($S_{TI} = 0$). Figure 17 shows that the values of $f_{Gr_{end}}$ decreased when the austenitizing temperature increased, because the austenite was able to receive more atoms of carbon from the graphite nodule.

Both $f_{\alpha p_{end}}$ and $f_{\gamma_{end}}$ depended mainly on the austenite temperature. Additionally, these fractions were affected by the austempering temperature, as it follows from the values of S_{Ti} in Table IV. Analyzing the index S_{Ii}, it is concluded that there was a very small interaction between these two thermal cycle parameters.

Changes in volume fractions of ferrite subunits and austenite, at the end of the heat treatment, are shown in scatter plots in Figures 18 and 19, respectively. When the austenitizing temperature increased, the ferrite subunit volume fraction decreased, because the austenite carbon content at the beginning of the austempering transformation increased. When the austempering temperature increased, the ferrite subunit volume fraction decreased, because the austenite carbon content decreased when the ausferritic transformation is completed. As was expected, the behavior of the austenite volume fraction was opposite to that of the ferrite subunit volume fraction. This occurs because the austenite was consumed by ferrite subunits during the

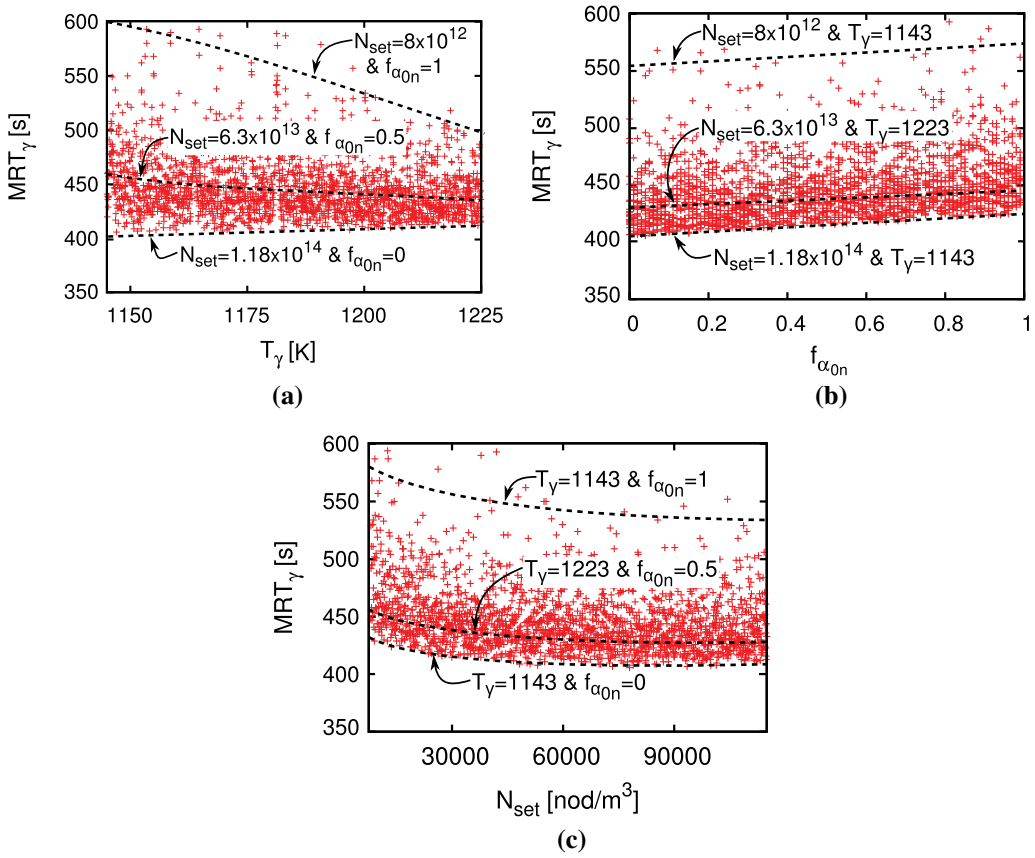

Fig. 11—Influence of (*a*) austenitizing temperature, (*b*) initial ferrite volume fraction, and (*c*) graphite nodule count on MRT_γ.

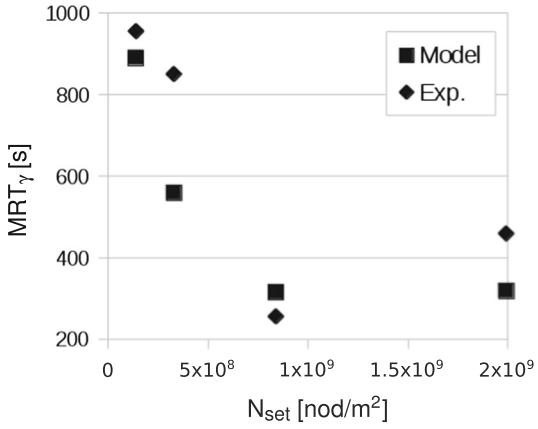

Fig. 12—Comparison of model and experimental results for the minimum required time MRT_γ for different values of graphite nodule count per unit of area.

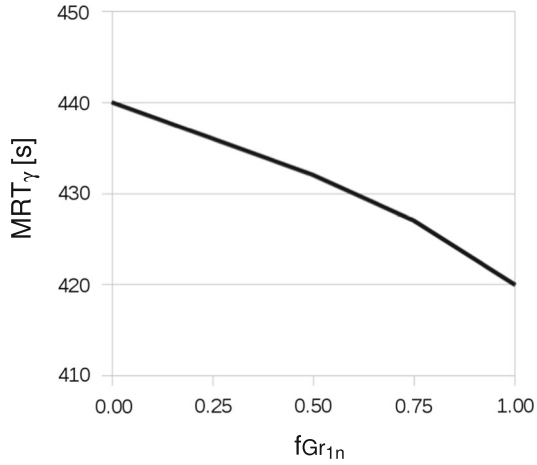

Fig. 13—Influence of normalized graphite volume fraction for set 1 on MRT_γ.

ausferritic transformation. The obtained results agree with results presented by Trudel and Gagné.[4]

Table VII summarizes the results of the sensitivity analyses. The input parameters that affect each analyzed output, its degree of influence, and the global behavior of the output are included.

VI. CONCLUSIONS

The analysis presented in this work identifies the process parameters that have a remarkable influence on the ADI microstructure obtained at the end of the heat treatment. The influence of process parameters, such as

Table V. S_{Ii} and S_{TI} Indices for the Analyzed Output

Output	S_{Ii}				S_{TI}
	$f_{\alpha_{0n}}$	N_{set}	T_γ	T_A	
MRT_γ	0.03	0.01	0.03	0.0	0.07
MRT_A	0.0	0.03	0.04	0.08	0.1
$f_{Gr_{end}}$	0.0	0.0	0.0	0.0	0.0
$f_{\alpha p_{end}}$	0.0	0.0	0.01	0.01	0.01
$f_{\gamma_{end}}$	0.0	0.0	0.01	0.01	0.0

Table VI. Values of Input Parameters for Different Cases Presented in Fig. 10

Case	N_{set} (nod/m^3)	$f_{\alpha_{0n}}$	T_γ $[K\ (°C)]$	T_A $[K\ (°C)]$
1	6.308×10^{13}	0.5	1183 (910)	638 (365)
2	9.064×10^{13}	0.25	1163 (890)	670.5 (397.5)
3	3.552×10^{13}	0.75	1203 (930)	605.5 (332.5)
4	7.686×10^{13}	0.12	1213 (940)	686.8 (413.8)

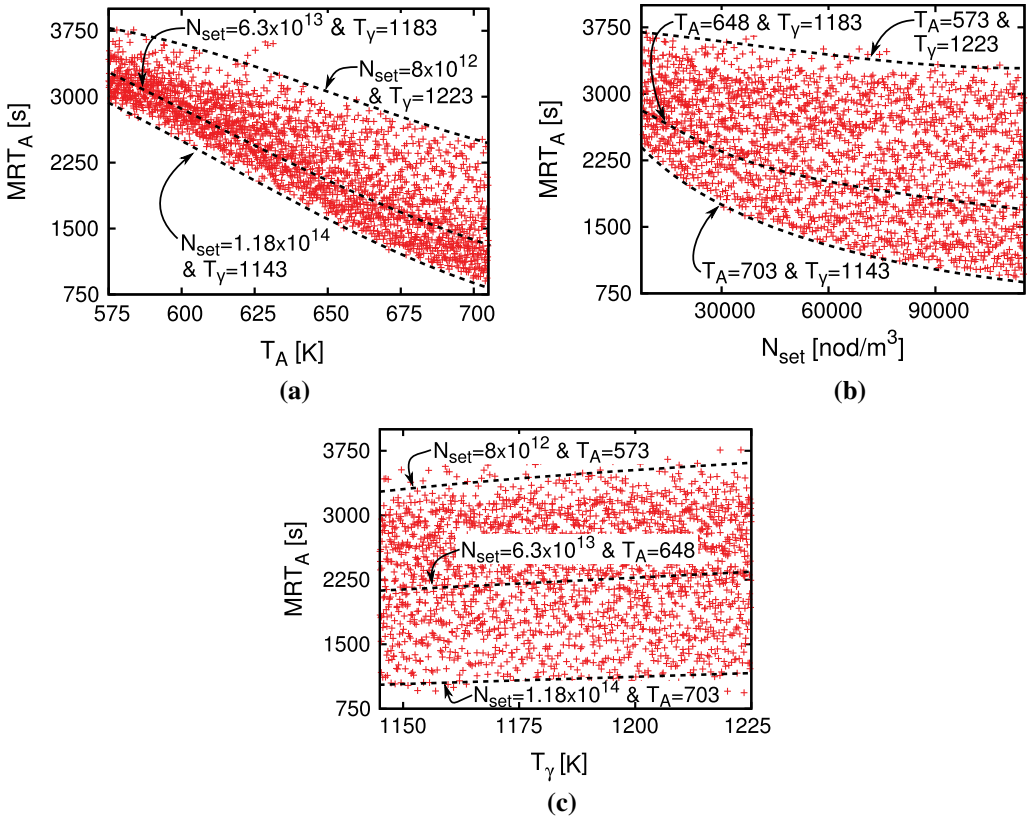

Fig. 14—Influence of (*a*) austempering temperature, (*b*) graphite nodule count, and (*c*) austenitizing temperature on MRT_A.

graphite nodule count, type of initial matrix, and austenitizing and austempering temperatures on MRT_γ, MRT_A, and phase fractions at the end of the heat treatment, was determined by means of both variance-based sensitivity analysis and scatter plot analysis. The database necessary to perform the analysis was obtained by numerical simulation of the three-step heat treatment using a coupled thermo-metallurgical model.

The main conclusions of this work may be summarized as follows:

1. When the shape and size of a DI part are kept constant, the minimum required time for the austenitization step depends on the austenitizing temperature (thermal

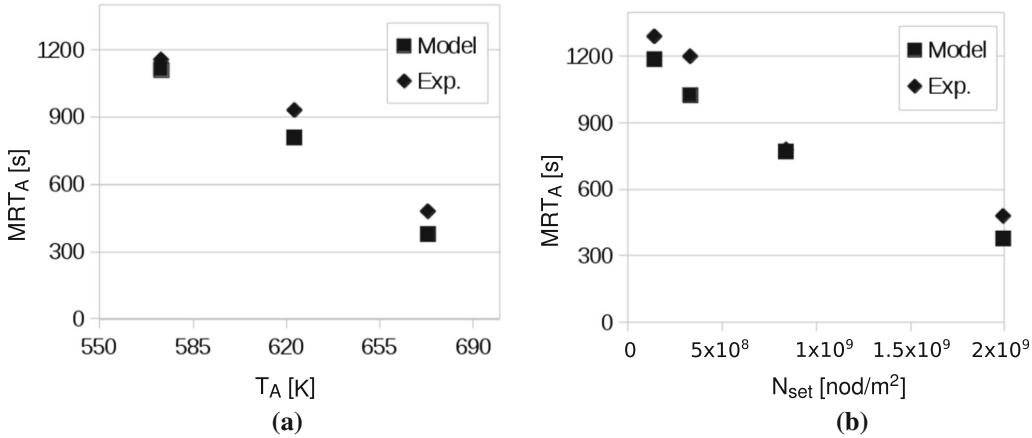

Fig. 15—Comparison of model and experimental results for the minimum required time MRT_A for different values of (*a*) austempering temperature and (*b*) graphite nodule count per unit of area.

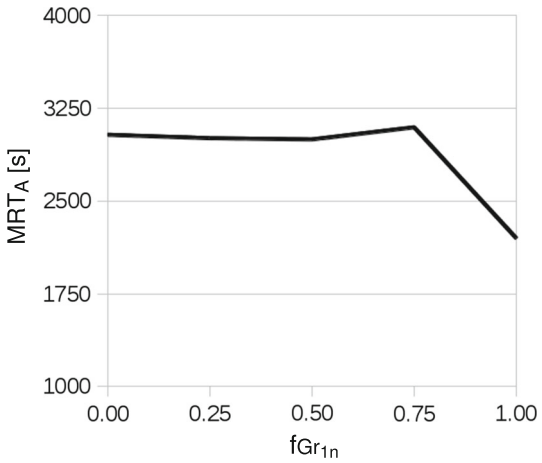

Fig. 16—Influence of normalized graphite volume fraction for set 1 on MRT_A.

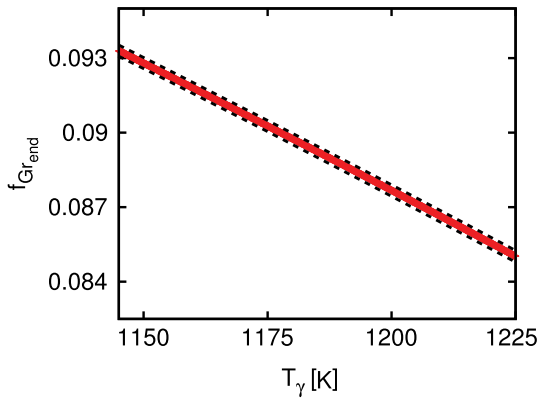

Fig. 17—Influence of austenitizing temperature on $f_{Gr_{end}}$.

Table VII. Summary of Sensitivity Analysis Results. The Symbols ↑ and ↓ Represent the Increment and Decrement of a Variable, Respectively

Output	Input Parameter	Degree of Influence	Global Behavior
MRT_γ	T_γ	high	$T_\gamma \uparrow MRT_\gamma \downarrow$
	N_{set}	low	$N_{set} \uparrow MRT_\gamma \downarrow$
	$f_{\alpha_{0n}}$	low	$f_{\alpha_{0n}} \uparrow MRT_\gamma \uparrow$
MRT_A	T_A	high	$T_A \uparrow MRT_A \downarrow$
	N_{set}	medium	$N_{set} \uparrow MRT_A \downarrow$
	T_γ	low	$T_\gamma \uparrow MRT_A \uparrow$
$f_{Gr_{end}}$	T_γ	high	$T_\gamma \uparrow f_{Gr_{end}} \downarrow$
$f_{\alpha p_{end}}$	T_γ	high	$T_\gamma \uparrow f_{\alpha p_{end}} \downarrow$
	T_A	medium	$T_A \uparrow f_{\alpha p_{end}} \downarrow$
$f_{\gamma_{end}}$	T_γ	high	$T_\gamma \uparrow f_{\gamma_{end}} \uparrow$
	T_A	medium	$T_A \uparrow f_{\gamma_{end}} \uparrow$

cycle parameter), and the graphite nodule count and type of initial matrix (initial microstructure parameters). MRT_γ is mainly influenced by the austenitizing temperature, and its global behavior is an increment of MRT_γ when T_γ decreases. Moreover, MRT_γ is weakly influenced by the graphite nodule count and type of initial matrix, and its global behavior is characterized by (a) an increment of MRT_γ when graphite nodule count decreases and (b) an increment of MRT_γ when the initial ferrite volume fraction increases.

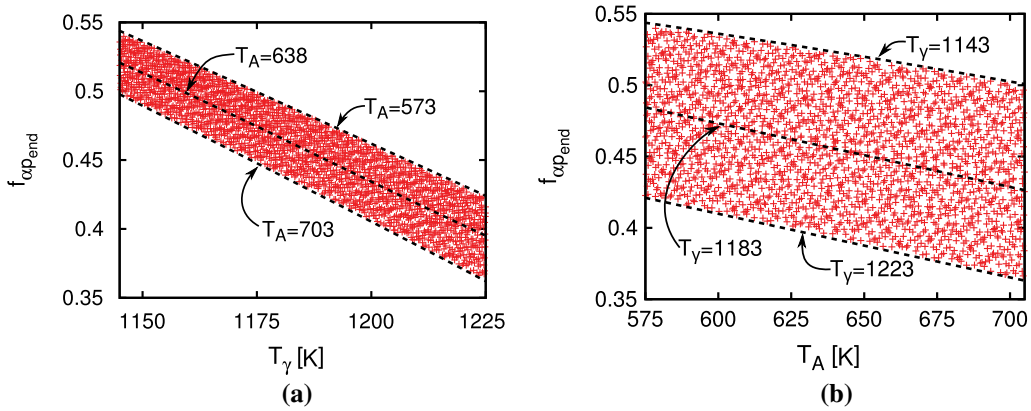

Fig. 18—Influence of (*a*) austenitizing temperature and (*b*) austempering temperature on $f_{\alpha p_{end}}$.

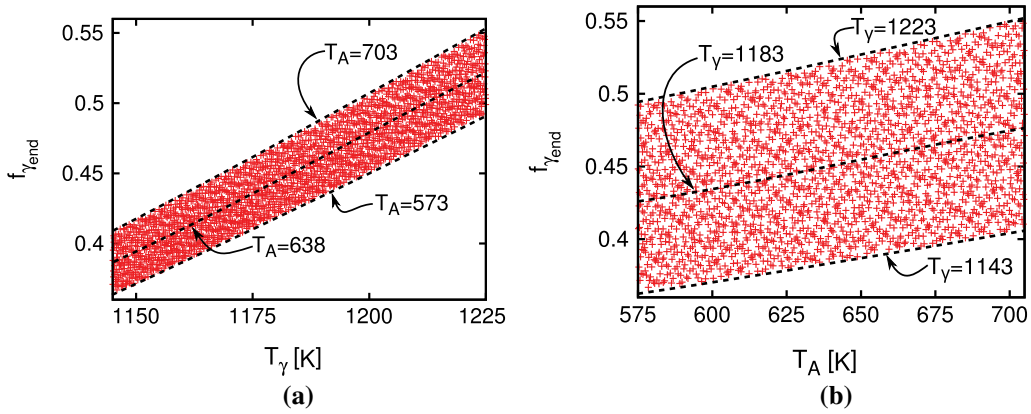

Fig. 19—Influence of (*a*) austenitizing temperature and (*b*) austempering temperature on $f_{\gamma_{end}}$.

2. When the shape and size of a DI part are kept constant, the minimum required time for the austempering step depends on the austenitizing and austempering temperatures (thermal cycle parameters) and the graphite nodule count (initial microstructure parameter). MRT_A is mainly influenced by the austempering temperature, and its global behavior is a increment of MRT_A when T_A decreases. The graphite nodule count has also a remarkable influence, increasing MRT_A when the value of N_{set} decreases. Finally, the influence of the austenitizing temperature is small, increasing MRT_A when T_γ increases.
3. When a part of DI is subjected to an austempering heat treatment in which the austenitization and austempering times satisfy the conditions $t_\gamma \geq MRT_\gamma$ and $t_A \geq MRT_A$, the final microstructure of the material depends on the austenitizing and austempering temperatures (thermal cycle parameters). This conclusion is valid if two additional conditions are satisfied: (a) the carbide precipitation starts, at the austempering temperature, at time $t \gg MRT_A$ and (b) the eutectoid transformation is avoided, throughout the part, during the cooling down from T_γ up to T_A. The graphite volume fraction depends only on the austenitizing temperature, increasing when the temperature decreases. The ferrite subunit volume fraction is mainly modified by the austenitizing temperature, and this fraction increases when the temperature decreases; it is also influenced by the austempering temperature, increasing when T_A decreases. The austenite volume fraction also depends on both the austenitizing and austempering temperatures. However, the global behavior is opposite to that of the ferrite subunit volume fraction.

The sensitivity analysis tool applied to a model that simulates a manufacture process has allowed identifying the influence of the process parameters. It is expected that the sensitivity analysis of parameters, such as chemical composition and geometry of the part, will also be considered within the present research program.

ACKNOWLEDGMENTS

A.D. Boccardo had a postdoctoral scholarship from CONICET during this research. P.M. Dardati was supported by a grant from UTN. L.A. Godoy is a member of the research staff of CONICET. D.J. Celentano acknowledges the support of CONICYT through REDES Project 150041.

REFERENCES

1. M.A. Yescas and H.K.D.H. Bhadeshia: *Mater. Sci. Eng. A*, 2002, vol. 333, pp. 60–66.
2. D.C. Putman and R.C. Thomson: *Int. J. Cast Met. Res.*, 2003, vol. 16, pp. 191–96.
3. U. Batra, S. Ray, and S.R. Prabhakar: *J. Mater. Eng. Perform.*, 2004, vol. 13, pp. 64–68.
4. A. Trudel and M. Gagné: *Can. Metall. Q.*, 1997, vol. 36, pp. 289–98.
5. B. Bosnjak, B. Radulovic, K. Pop-Tonev, and V. Asanovic: *J. Mater. Eng. Perform.*, 2001, vol. 10, pp. 203–11.
6. E. Fraś, M. Górny, E. Tyrała, and H. Lopez: *Mater. Sci. Technol.*, 2012, vol. 28, pp. 1391–96.
7. M. Ji and R. Shivpuri: *Mater. Sci. Eng. A*, 2006, vol. 425, pp. 156–66.
8. J.S. Sun and C.S. Wu: *Model. Simul. Mater. Sci.*, 2001, vol. 9, pp. 25–36.
9. S.D. Ji, H.Y. Fang, X.S. Liu, and Q.G. Meng: *Model. Simul. Mater. Sci.*, 2005, vol. 13, pp. 553–65.
10. S. Karaoğlu and A. Seçgin: *J. Mater. Process. Tech.*, 2008, vol. 202, pp. 500–07.
11. Z. Peng and T. Sheppard: *Model. Simul. Mater. Sci.*, 2004, vol. 12, pp. 43–57.
12. S. Hansson and T. Jansson: *J. Mater. Process. Tech.*, 2010, vol. 210, pp. 1386–96.
13. S.K. Fjeldbo, Y. Li, K. Marthinsen, and T. Furu: *J. Mater. Process. Tech.*, 2012, vol. 212, pp. 171–80.
14. P. Ferro: *Model. Simul. Mater. Sci.*, 2012, vol. 20, art. 085003.
15. A. Kumar, M. Založnik, H. Combeau, B. Goyeau, and D. Gobin: *Model. Simul. Mater. Sci.*, 2013, vol. 21, art. 045016.
16. E. Hepp, V. Hurevich, and W. Schäfer: *IOP Conf. Ser-Mat. Sci.*, 2012, vol. 33, art. 012076.
17. A.D. Boccardo, P.M. Dardati, D.J. Celentano, L.A. Godoy, M. Górny, and E. Tyrała: *Mater. Trans. B*, 2016, vol. 47, pp. 566–75.
18. A.D. Boccardo, P.M. Dardati, D.J. Celentano, and L.A. Godoy: *Finite Elem. Anal. Des.*, 2017, vol. 134, pp. 82–91.
19. D.J. Celentano: *Int. J. Plast.*, 2001, vol. 17, pp. 1623–58.
20. D.J. Celentano: *Mater. Manuf. Process.*, 2010, vol. 25, pp. 546–56.
21. D.J. Celentano, P.M. Dardati, F.D. Carazo, and L.A. Godoy: *Mater. Sci. Technol.*, 2013, vol. 29, pp. 156–64.
22. R.M. Ghergu, J. Sertucha, Y. Thebault, and J. Lacaze: *ISIJ Int.*, 2012, vol. 52, pp. 2036–41.
23. H.K.D.H. Bhadeshia: *Bainite in Steels*, 2nd ed., IOM Communications, London, 2001.
24. A.D. Boccardo, P.M. Dardati, D.J. Celentano, and L.A. Godoy: *Mater. Trans. A*, 2017, vol. 48, pp. 524–35.
25. A. Saltelli, M. Ratto, T. Andres, F. Campolongo, J. Cariboni, D. Gatelli, M. Saisana, and S. Tarantola: *Global Sensitivity Analysis: The Primer*, Wiley, England, 2008, pp. 155–82.
26. A. Saltelli, P. Annoni, I. Azzini, F. Campolongo, M. Ratto, and S. Tarantola: *Comput. Phys. Commun.*, 2010, vol. 181, pp. 259–70.
27. I.M. Sobol' and Y.L. Levitan: *Comput. Math. Appl.*, 1999, vol. 37, pp. 33–40.
28. A.D. Boccardo: *Thermo-Mechanical-Metallurgical Modelling of Austempering Heat Treatment of Ductile Irons (in Spanish)*, PhD Thesis, Universidad Nacional de Córdoba, Córdoba, Argentina, 2017, http://hdl.handle.net/11086/4758.
29. J. Lacaze and V. Gerval: *ISIJ Int.*, 1998, vol. 38, pp. 714–22.
30. W. Kapturkiewicz, E. Fraś, and A.A. Burbelko: *Mater. Sci. Eng. A*, 2005, vols. 413–414, pp. 352–57.